

The TACTIC atmospheric Cherenkov Imaging telescope

R. Koul, A.K. Tickoo^{*}, S.K. Kaul, S.R. Kaul, N. Kumar, K.K. Yadav, N. Bhatt, K. Venugopal, H.C. Goyal, M. Kothari, P. Chandra, R.C. Rannot, V.K. Dhar, M.K. Koul, R.K. Kaul, S. Kotwal, K. Chanchalani, S. Thoudam, N. Chouhan, M. Sharma, S. Bhattacharyya, S. Sahayanathan

*Bhabha Atomic Research Centre,
Astrophysical Sciences Division.
Mumbai - 400 085, India.*

Abstract

The TACTIC γ -ray telescope, equipped with a light collector of area $\sim 9.5\text{m}^2$ and a medium resolution imaging camera of 349-pixels, has been in operation at Mt. Abu, India since 2001. This paper describes the main features of its various subsystems and its overall performance with regard to (a) tracking accuracy of its 2-axes drive system, (b) spot size of the light collector, (c) back-end signal processing electronics and topological trigger generation scheme, (d) data acquisition and control system and (e) relative and absolute gain calibration methodology. Using a trigger field of view of 11×11 pixels ($\sim 3.4^\circ \times 3.4^\circ$), the telescope records a cosmic ray event rate of ~ 2.5 Hz at a typical zenith angle of 15° . Monte Carlo simulation results are also presented in the paper for comparing the expected performance of the telescope with actual observational results. The consistent detection of a steady signal from the Crab Nebula above ~ 1.2 TeV energy, at a sensitivity level of $\sim 5.0\sigma$ in ~ 25 h, alongwith excellent matching of its energy spectrum with that obtained by other groups, reassures that the performance of the TACTIC telescope is quite stable and reliable. Furthermore, encouraged by the detection of strong γ -ray signals from Mrk 501 (during 1997 and 2006 observations) and Mrk 421 (during 2001 and 2005-2006 observations), we believe that there is considerable scope for the TACTIC telescope to monitor similar TeV γ -ray emission activity from other active galactic nuclei on a long term basis.

Key words: Gamma-ray astronomy, Cherenkov imaging, TACTIC telescope.
PACS: 95.55.Ka;29.90.+r

^{*} Corresponding author :

Email address: aktickoo@barc.gov.in (A.K. Tickoo).

1 Introduction

Gamma-ray photons in the very high energy range (0.1 - 50 TeV) are expected to come from a wide variety of cosmic objects from, both, within and outside the Milky Way Galaxy. The candidate sources include supernova remnants [1,2], OB star associations [3], X-ray binary systems [4,5] and active galactic nuclei [6]. Studying this radiation in detail can yield valuable and, quite often, unique information about the unusual astrophysical environment characterizing these sources, as also on the intervening intergalactic space [7]. Whileas this promise of the cosmic TeV γ -ray probe has been appreciated for quite a long time, it was the landmark development of the 'imaging' technique and the principle of 'stereoscopic imaging', proposed by the Whipple [8] and the HEGRA [9] groups, respectively, that revolutionized the field of ground-based very high energy γ -ray astronomy. In this technique, the spatial distribution of the photons in the image plane (called the Cherenkov image) is recorded by using a close-packed array of fast photomultiplier tubes (also called the Imaging Camera with individual PMTs as its pixels). Detailed Monte-Carlo simulation studies have shown that the Cherenkov images resulting from γ -ray showers from a point source are compact and roughly elliptical in shape with their major axis pointing towards the source direction in the focal plane camera [10,11]. On the contrary, Cherenkov images resulting from cosmic ray showers are broader in size, irregular in their shape and, are randomly oriented in the focal plane due to their isotropic nature. Modern atmospheric Cherenkov telescopes (e.g MAGIC [12], VERITAS [13], HESS [14] and CANGAROO [15]), utilizing the 'imaging' technique, allow the removal of more than 99.5 % of the cosmic-ray background, yielding an unprecedented sensitivity in the TeV energy range.

The TACTIC (TeV Atmospheric Cherenkov Telescope with Imaging Camera) γ -ray telescope [16] has been in operation at Mt. Abu (24.6° N, 72.7° E, 1300m asl), India, for the last several years to study TeV gamma ray emission from celestial sources. The telescope uses a tessellated light-collector of area $\sim 9.5\text{m}^2$ which is capable of tracking a celestial source across the sky. The telescope deploys a 349-pixel imaging camera, with a uniform pixel resolution of $\sim 0.3^\circ$ and a $\sim 6^\circ \times 6^\circ$ field-of-view, to take a fast snapshot of the atmospheric Cherenkov events produced by an incoming cosmic ray particle or a gamma ray photon with an energy above $\sim 1\text{TeV}$. The photographs of the TACTIC imaging telescope and its back-end signal processing electronics are shown in Fig.1 In this paper, we discuss the instrumentation aspects of the TACTIC imaging element. Apart from giving the basic description, the present paper provides a quantitative performance of its hardware comprising light collector optics, drive control system, front-end and back-end instrumentation. Finally, the system performance will be evaluated through the analysis of TeV γ -ray observations of the Crab Nebula and Mrk 421.

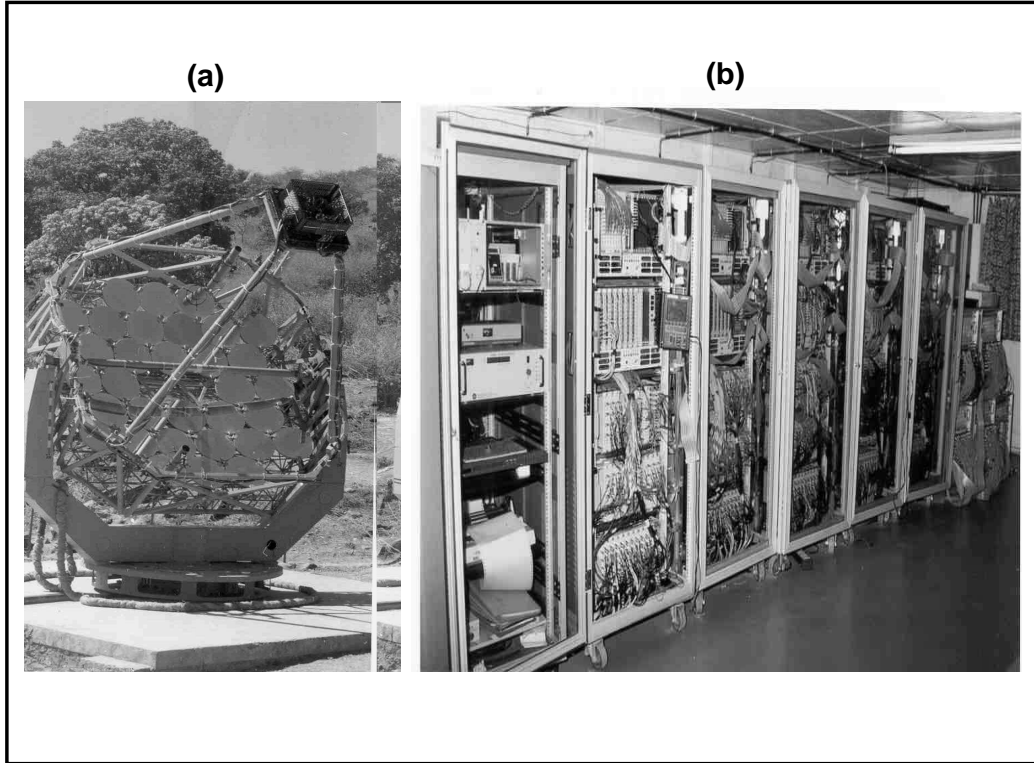


Fig. 1. (a) Photograph of the 349-pixel TACTIC imaging telescope (b) Photograph of back-end signal processing electronics used in the telescope.

2 Observatory Site

Keeping in mind the overall scientific requirements of a good astronomical site for atmospheric Cherenkov systems, a comprehensive site survey program was undertaken by us in 1993 [17] and Mt.Abu (24.63°N , 72.75°E , 1300m asl), a hill resort in Western Rajasthan (India) was found to be an excellent location in the country for setting up the TACTIC telescope. The main reasons for choosing Mt.Abu as the site for TACTIC telescope are that it offers: (a) Maximum number of cloud free nights during a calendar year, (b) Reasonably dark site, with a negligible contribution to the background light level from artificial sources, (c) Haze, dust and pollution free atmosphere. (d) Operational ease, good logistics and mild climate. The INSAT-1D satellite cloud cover images in the infrared (10500-12500 nm) and visible (550-700 nm) bands were studied to derive quantitative information on the percentage of clear nights per year. An analysis of the 5-year data (1986-1991), revealed that the mean percentage of clear nights at Mt. Abu is the highest, among the 7 potential sites explored, translating to about 1170 hours per year of effective observations for atmospheric Cherenkov work [17]. The monthly distribution of this observation time available at Mt. Abu is essentially uniform, except for the monsoon-affected months of June-September. Dust loads of about $20 \mu\text{g m}^{-3}$, precipitable water vapour content of only a few mm during non-monsoon period and peak wind-

speeds of 60 km h^{-1} are some other relevant parameters of the selected site. The extinction measurements carried out at Mt.Abu over the spectral band $\sim 310\text{-}560$ nm lead to mean extinction coefficient of $\sim 0.47 \pm 0.10$ and $\sim 0.31 \pm 0.07$ for the pre-monsoon and post-monsoon period, respectively, to be compared with a value of ~ 0.35 at Mt.Abu altitude for a standard atmosphere. The mean night sky brightness levels during the two observation spells were found to be $\sim (1.34 \pm 0.50) \times 10^{12}$ photons $\text{m}^{-2}\text{s}^{-1}\text{sr}^{-1}$ (pre-monsoon) and $\sim (1.54 \pm 0.55) \times 10^{12}$ photons $\text{m}^{-2}\text{s}^{-1}\text{sr}^{-1}$ (post-monsoon).

3 Mechanical structure of the telescope

The main sub-assemblies of the TACTIC telescope are : mirror basket, mirror fixing/adjusting frames, zenithal and azimuthal gear assembly, encoders/motors for its two axes, camera support boom assembly and the photomultiplier tube-based imaging camera. A three dimensional truss type structure has been used to support the mirror frame. The mirror basket is a 3 layer welded mildsteel tubular grid structure fabricated in 3 parts which are bolted together. The basket is provided with a central tie rod which extends into short stub shafts at the two ends which are housed in bearings. The individual mirror facets (34 in number, each with a diameter 60 cm and weighing around 20 kg) are supported on three levelling studs, so that desired inclination of the specific mirror with respect to the telescope axis can be achieved. The weight of the moving part of the telescope is around 6.5 t. The complete basket assembly is held by the fork of the telescope which transmits the load through the central roller thrust bearing to the telescope foundation. The horizontal part of the fork frame is clamped on to a large gear of the azimuthal drive rotary table of the telescope. The thrust bearing using hardened rollers was specially designed and fabricated in-house. A central pin and a taper roller bearing, housed in the large gear is used to ensure proper rotation about its vertical axis. The base structure has been anchored to the ground by 4 foundation bolts. The zenithal motion to the telescope is given from only one end of the basket. A common shaft assembly fixed in self aligning ball bearing having a large gear fixed on it, provides the zenithal rotation of the mirror basket. Five stage gear box providing a total speed reduction of 5189.14 has been used in the zenithal drive of the telescope. Likewise, a four stage gear box leading to a speed reduction of 6348.94 has been used in the azimuth drive. A large capacity circular cable drag chain has been provided for easy and free movement of the nearly 700 signal and high voltage cables.

Deflection analysis using FEM software package has also been performed at various zenith angles to arrive at the shift in the focal point position due to structural deformations of the mirror basket frame, mirror holding attachment and support booms. The results of this study indicate that a shift of $< 3\text{mm}$ in the focal point position can be produced over the zenith angle range of 0^0 to 70^0 .

4 Drive control system

The need for using a large light collector aperture ($\sim 3.5\text{m}$) and the attendant large telescope weight ($\sim 6.5\text{ t}$) have led to the choice of an altitude-azimuth (alt-azm) mounting for the TACTIC telescope, as against the comparatively simpler equatorial mounting. The main advantage of the alt-azm mount is that the telescope weight is supported uniformly on a horizontally-placed central thrust-bearing. Fig.2 depicts the block diagram of the TACTIC drive control system whose design is based on the CAMAC standard. It uses hybrid stepper motors, sequence generators and power amplifiers, 16-bit absolute shaft-encoders, programmable stepper motor controllers and a GPS clock. Two CAMAC-compatible, 24-bit input registers have

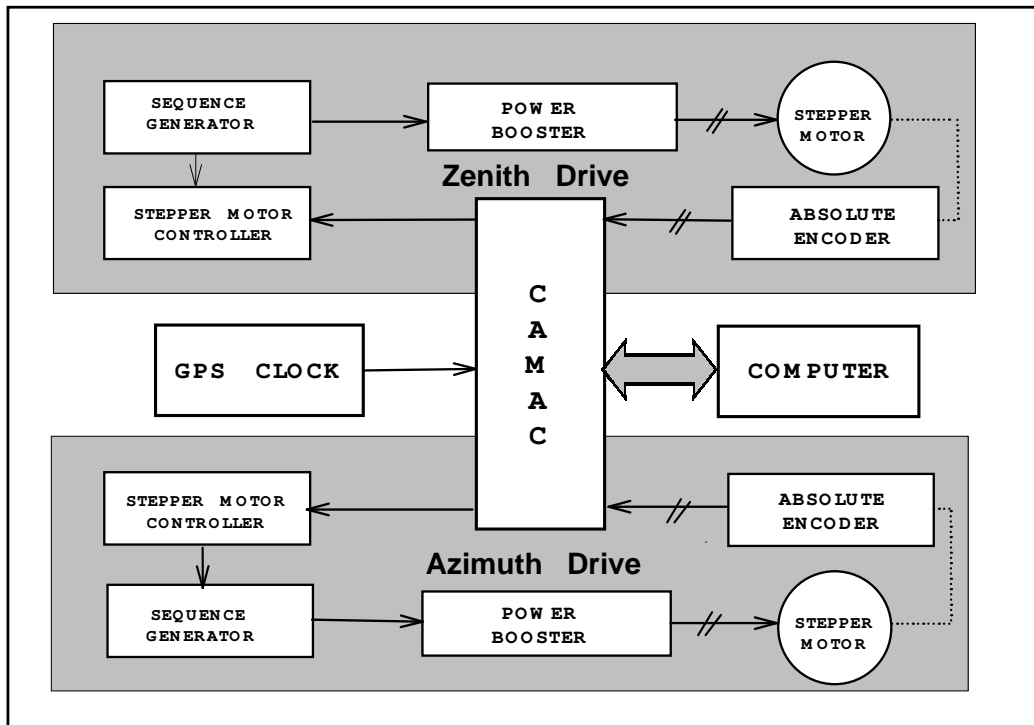


Fig. 2. Block diagram of the TACTIC telescope drive control system.

been used to input the telescope zenith and azimuth information to the drive system computer to enable its control software to work in a closed-loop configuration with absolute shaft encoders monitoring the azimuth and zenith angles of the telescope and the corresponding stepper motors providing the movement of its axes.

The drive torque including a reasonable safety factor of ~ 2 , required to overcome the counteracting frictional and inertial torques and for smoothly moving the azimuthal drive at the maximum specified acceleration of 2 arc-min s^{-2} , has been calculated to be about 80 N cm . This value has been estimated on the basis of the expected moment of inertia of the various moving components of the telescope and rather conservative estimates of the coefficient of friction for the bearing used. The

TACTIC telescope uses two 100 N cm hybrid stepper motors (Pacific Scientific make, Model H 31NREB, NEMA Size 34) for driving its azimuthal and zenithal axes through multistage gear-trains. The motors have a step size of 1.8° and are used in the 'full-step' mode. The speed and direction control for each axis of the telescope is implemented through an in-house developed CAMAC-based Stepper Motor Controller module which provides a programmable output clock of any desired frequency between 0.15 Hz and 3kHz. A Sequence Generation Module, based on the unipolar full-step switching pattern, routes the input pulses to the appropriate switches of the chopper-based power booster. The maximum azimuthal speed of the TACTIC telescope is 100 rad/rad (equivalent to $1500^\circ \text{ h}^{-1}$), and the resulting blind spot has a diameter $\sim 1.2^\circ$. Single turn Resolver-based 16-bit absolute shaft encoders (Computer Conversion Corporation make; NEMA 12), with a resolution of ± 0.33 arc-min and the worst case accuracy of ± 6 arc-min, are used for monitoring the orientation of the telescope. The two resolvers, coupled to 16-bit resolution decoders, were calibrated on a precision indexing table (resolution ~ 0.5 arc-sec; accuracy ~ 5 arc-sec) and it was found that the error profiles are largely of systematic nature [18]. Accordingly, a software-based procedure has been successfully developed for compensating for this systematic error-profile of the encoders. A GPS based CAMAC-compatible digital clock (Hytec Electronics Ltd. make; GPS92) with a resolution of ~ 10 ns and absolute time accuracy of ~ 100 ns, is used to compute the source co-ordinates in real time. The new co-ordinates of the source are calculated after every second while tracking a candidate source. More details regarding various hardware components of the telescope drive system are discussed in [19].

The user friendly in-house developed tracking system software provides an independent movement for the zenithal and azimuthal axes so that a matching between the telescope pointing direction and the source direction is obtained with an accuracy better than ± 2 arc-min. Once the error goes outside the permissible bounds of ≤ 2 arc-min in case of either axis, at a zenith angle $\geq 7^\circ$, a correction cycle (in the form of temporary halt or faster movement at a stepping rate of ~ 100 Hz) is applied till the corresponding offset gets restored to within ≤ 1.0 arc-min. While this on-off type of correction cycle works perfectly for correcting the zenithal error, irrespective of the source declination, following the same principle in the azimuth axis works properly for only those sources which have a minimum zenith angle of 7° . For sources which have a minimum zenith angle in the range $2^\circ - 7^\circ$, we have provided for ramp-up correction cycle (with stepping rates upto 400 Hz), for tracking them close to their upper transit, to avoid the problem of indefinite chase which would have otherwise occurred if the correction was performed at a stepping rate of 100 Hz. Furthermore, since an azimuth error upto ~ 15 arc-min can be easily tolerated at a typical zenith angle of around 3° without leading to any serious deterioration in the pointing direction of the telescope, the permissible azimuth error band has been accordingly dynamically widened from ~ 2 arc-min to ~ 15 arc-min, depending on the zenith angle of the source, so that frequent correction cycles leading to a possible 'hunting' problem can be avoided. Fig.3 gives the rep-

representative error profiles in the zenith, azimuth and pointing angles of the telescope during tracking of the Crab Nebula (declination $\sim 22.014^\circ$; zenith angle $\sim 2.6^\circ$ at upper transit) for ~ 5 hours. Furthermore, since the TACTIC telescope uses a single-

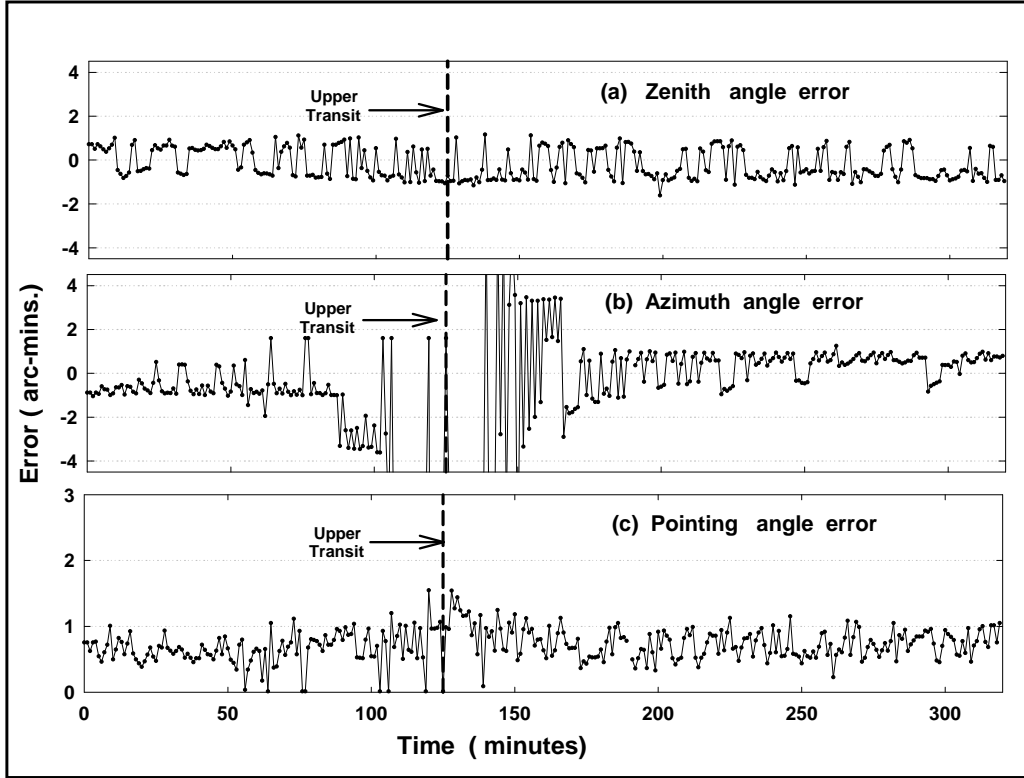


Fig. 3. Representative error-profiles in the zenith (a), azimuth (b) and pointing (c) angles of the TACTIC telescope, obtained while tracking the Crab Nebula (declination $\sim 22.014^\circ$; zenith angle $\sim 2.6^\circ$ at upper transit) for ~ 6 h. It is worth pointing out that despite encountering large azimuth error (i.e around time ~ 125 minutes in the figure when the source is close to its upper transit), because of the inherent characteristics of the alt-azm drive, the error in the pointing direction of the telescope is still within tolerable limits of ~ 2 arc-min.

ended drive on both axes, a correction cycle involving a fast movement along with change of direction has been deliberately avoided unless it is genuinely required for a source, to overcome the problem of back-lash error.

The tracking accuracy of the telescope is also checked on a regular basis with so called 'point runs', where a reasonably bright star, having a declination close to that of the candidate γ -ray source is tracked continuously for about 5 hours. The point run calibration data (corrected zenith and azimuth angle of the telescope when the star image is centered) are then incorporated in the telescope drive system software so that appropriate corrections can be applied directly in real time while tracking a candidate γ -ray source.

5 Light-collector design of the TACTIC telescope

The TACTIC light-collector with a collection area of $\sim 9.5\text{m}^2$ uses 34 front-face aluminium-coated, glass spherical mirrors of 60cm diameter each with the following characteristics (i) focal length $\sim 400\text{cm}$, (ii) surface figure $\sim \text{few } \lambda$ (iii) reflection coefficient $>80\%$ at a wavelength of $\sim 400\text{nm}$ and (iv) thickness 20mm to 40mm. Fig.4a shows the projection of the mirror layout onto a plane transverse to the symmetry axis of the basket. The shorter focal length facets are deployed close to the principal axis of the basket while the longer focal length facets are deployed around the periphery. The peripheral mirrors have the effect of increasing the overall spot size as they function in an off-axis mode. In order to make the design as close to the Davies-Cotton design as possible, we used longer studs on the mirror frame structure to raise the pole positions of the peripheral mirrors numbered 18, 20, 26, 28, 31, 32, 33 (shown as shaded circles in Fig.4a). Fig.4b shows the measured reflection coefficients of individual mirrors. The reflection coefficient measurements of the mirrors were made using a reflectometer (Dyn-Optics make; Model 262). The reflectometer uses an electronically-chopped LED-based polychromatic light source with a bell shaped spectral distribution extending from 430 nm to 620 nm and having a peak emission at 550nm. Since the reflection coefficient measurement involves touching the mirror surface with a 2mm diameter bifurcated non-scratching fibre optic probe over a very small portion of the mirror being tested, we have used 7 randomly selected locations on the mirror surface to quantify the mean reflection coefficient of the mirror. The error bars shown in Fig.4b represent standard dispersion (1σ value) of the 7 reflection coefficient values.

The alignment of the various mirror facets is done by a two step process. In the first step, the orientation angle and the focal distance of the mirror facet pole is precalculated from geometrical considerations and the orientation of the mirror to within an error of $\sim 1^\circ$ is adjusted using a dummy facet at all the locations. The orientation of the dummy facet is set by adjusting the 3 ball-joints which couple the triangular mirror holding frame to the mirror basket. In the second step, the individual mirror facets of the telescope are further aligned precisely using an indigenously developed laser plumb-line. With telescope pointed in the vertical direction, an individual mirror facet is installed at its pre-designated location and the laser plumb line is suspended over it. The mirror facet is then slowly adjusted such that the reflected beam hits the centre of the focal plane. This fine adjustment is done by varying the gaps at the 3 locations below the mirror facet where it rests on the triangular holding frame. The above procedure is repeated for a total of 5 points on each mirror and these preselected points are the pole of the mirror facet and four equidistant points on the periphery of the mirror. Using this technique for all the mirror facets, one at a time, a common focus with the minimum possible image spread was obtained at a focal plane distance of 386cm instead of at 400cm, as would have been expected for a standard paraboloid or a Davies-Cotton design of the reflector. This value of focal plane distance was chosen on the basis of the

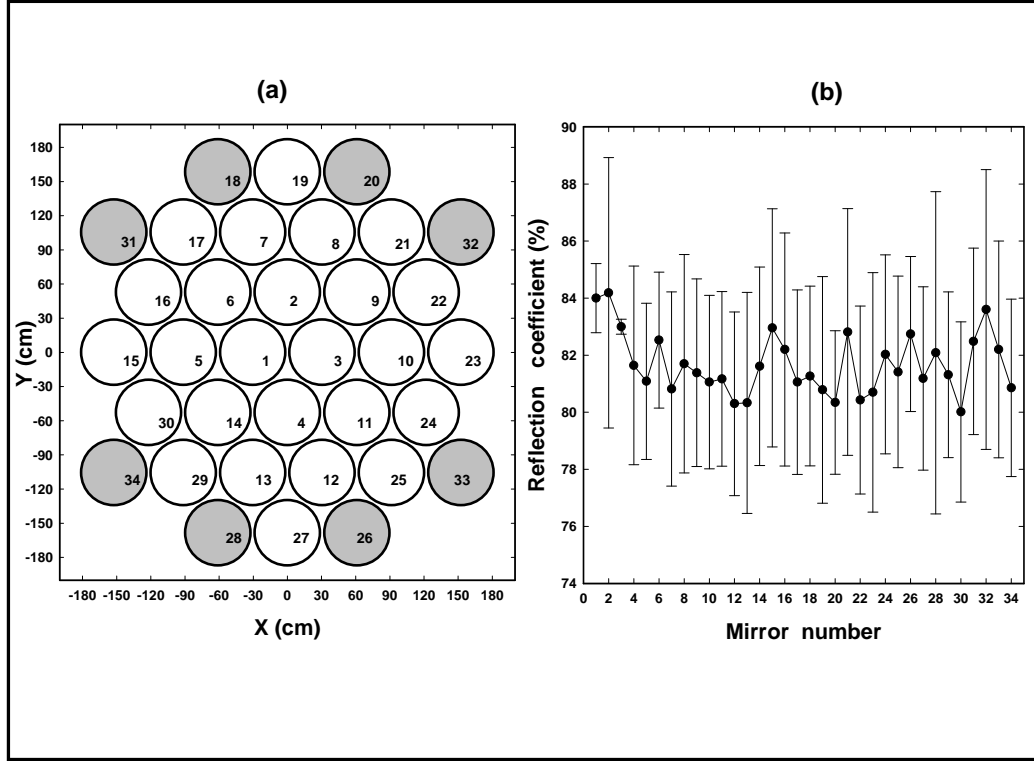


Fig. 4. (a) Projection of the 34 mirror facets of the tessellated light collector of the TACTIC telescope. The shaded circles represent the peripheral mirrors (labelled as 18, 20, 26, 28, 31, 32, 33 and 34) that have been raised along the z-axis of the light collector for obtaining a better point spread function. (b) Reflection coefficients for all the 34 mirrors used in the telescope.

simulation results [20]. The alignment of the mirror facets is further confirmed by observing a bright star image at the focal plane. Gross misalignment in any of the facets is easily identified as it results in multiple images being seen on the focal plane.

In order to evaluate the optical quality of the light collector experimentally, the telescope was pointed towards the bright star ζ -Tauri and its image recorded by monitoring the anode current of the central pixel of the imaging camera. The anode current versus angular offset plot is shown in Fig.5a. The point-spread function shown has a FWHM of $\sim 0.185^\circ$ ($\equiv 12.5\text{mm}$) and $D_{90} \sim 0.34^\circ$ ($\equiv 22.8\text{mm}$). Here, D_{90} is defined as the diameter of circle, concentric with the centroid of the image, within which 90% of reflected rays lie. An image of the star Sirius recorded at the focal plane of the telescope has also been shown in Fig.5b and it has superimposed on it two circles which correspond to the diameter of the pixel and measured D_{90} value calculated on the basis of Fig.5a. The value of $D_{90} \sim 0.29^\circ$ ($\equiv 19.3\text{mm}$), predicted on the basis of the simulation for an incidence angle of 0° , matches reasonably well with the measured value mentioned above. Other details regarding the ray-tracing simulation procedure and comparison of the measured point-spread

function of the TACTIC light collector with the simulated performance of ideal Davies-Cotton and paraboloid designs are discussed in [20].

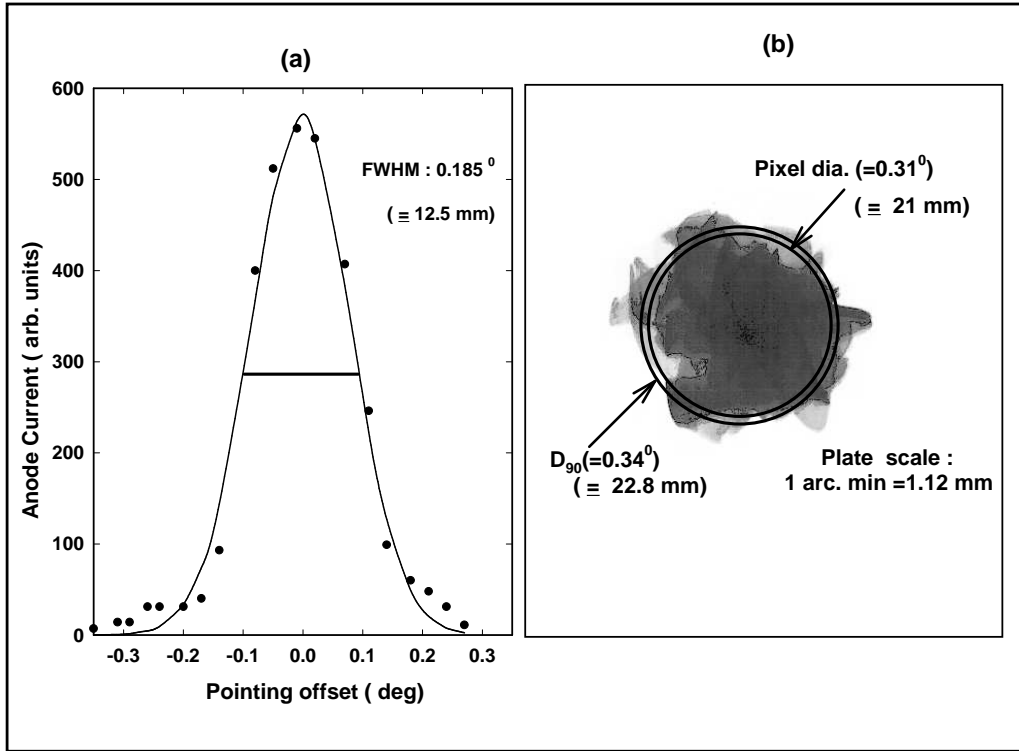


Fig. 5. (a) Measured point spread function of the TACTIC telescope light collector. (b) Photograph of the image produced by Sirius. Circles superimposed on the image have diameters $\sim 0.31^\circ$ and $\sim 0.34^\circ$ and represent the diameter of the camera pixels and D_{90} , respectively.

6 The imaging camera

6.1 Camera design

The 0.3° resolution imaging camera has been designed as a square grid arrangement which can be fabricated with ease. The camera frame is made up of two 5mm thick aluminium plates in which 19mm diameter holes are drilled at a pitch of 22mm corresponding to the locations of the 349 pixels. The photomultiplier tube is held in place by a metallic collar fixed to its socket which in turn is held to the rear plate by a specially designed fastener. Teflon O-rings isolate the glass window of the PMT from the metallic front plate. The pixels are divided into four sections with each section assigned to the connector panels on one particular side of the camera. This

arrangement allows quick identification and replacement of malfunctioning pixels. The central pixel of the camera which is on the principal axis of the light collector is used for checking the alignment of the mirror facets and the tracking/pointing accuracy of the telescope. The pixels are numbered sequentially clockwise from the central pixel which is designated as 1. This arrangement has the advantage of not disturbing the numbering subsequently as the number of operating pixels was increased from 81 in 1997 to 349 in the year 2001. The camera mounting system has a provision of varying its distance from the mirror basket by about ± 20 cm which is very useful in optimizing the focal plane distance for obtaining the best possible point spread function.

6.2 *Photomultiplier tubes and light guides*

The imaging camera uses 19mm diameter photomultiplier tubes (ETL-9083 UVB). The alkali photocathode has a maximum quantum efficiency of $\sim 27\%$ at 340nm and the use of UV glass for the window has enhanced its sensitivity in the 280-300nm wavelength band. The 10 stage linear focussed photomultiplier tube (PMT) has a rise time of ~ 1.8 ns which is compatible with the time profile of the Cherenkov pulse. A low current zener diode-based voltage divider network (VDN) is used with the PMT. This VDN design [21] has the advantage of ensuring stable voltages at the last two dynodes with VDN current of only about $240\mu A$ which is a factor of 5 less than the minimum current recommended for a resistive VDN. Low thermal dissipation is an important parameter for the stable operation of the multi-pixel camera. The VDN uses negative voltage and the photocathode is at a high voltage of 1000-1400V while the anode is at the ground potential. The VDN of the PMT is permanently soldered to its socket and two RG174 coaxial cables from each VDN circuit board are terminated with coaxial connectors on the connector panels fixed to 4 sides of the camera. The high voltage cable has a plug type SHV connector, while the signal cable uses a BNC connector thereby preventing the possibility of wrong connections.

The Compound Parabolic Concentrator (CPC) shape was chosen for the light guides to ensure better light collection efficiency and reduction in the background light falling on the photomultipliers. After prolonged trials with various materials the light guides were made of SS-304. These light guides were cut out of rods using a numerically controlled lathe which had the calculated profile details stored in it. Some of the important geometrical parameters of the CPCs used in the TACTIC telescope camera are the following : entry aperture ~ 21.0 mm; exit aperture ~ 15.0 mm; acceptance angle $\sim 45.58^\circ$ and height ~ 17.6 mm. The light collection of the CPC, which includes both the geometrical collection efficiency and the reflectivity of the surface was experimentally measured to be $\sim 65\%$.

7 Backend signal processing electronics and trigger generation

7.1 Signal processing electronics

The image of a typical atmospheric Cherenkov event is registered in the form of varying amplitude pulses of $\sim 3\text{mV} - 60\text{mV}$ produced by a group of 5-20 pixels of the camera. These voltage pulses are brought to the control room, using 55m long high quality RG 58 coaxial cables. In-house developed fast NIM Hex amplifier modules with a user selectable gain range of 2-50 and amplitude discriminator modules of 50 -500mV range are used for amplification and threshold selection of the PMT signals. While the multichannel fast NIM-based amplifier and fixed threshold discriminator modules have front panel adjustments for gain and threshold respectively, the charge content and the scaler rates are directly read off the CAMAC bus. The complete back end instrumentation (Fig.6) based on inhouse developed medium channel density modules is housed in seven 19 inch racks of 36 U height (Fig. 1b). One of the two outputs of a discriminator channel is used for

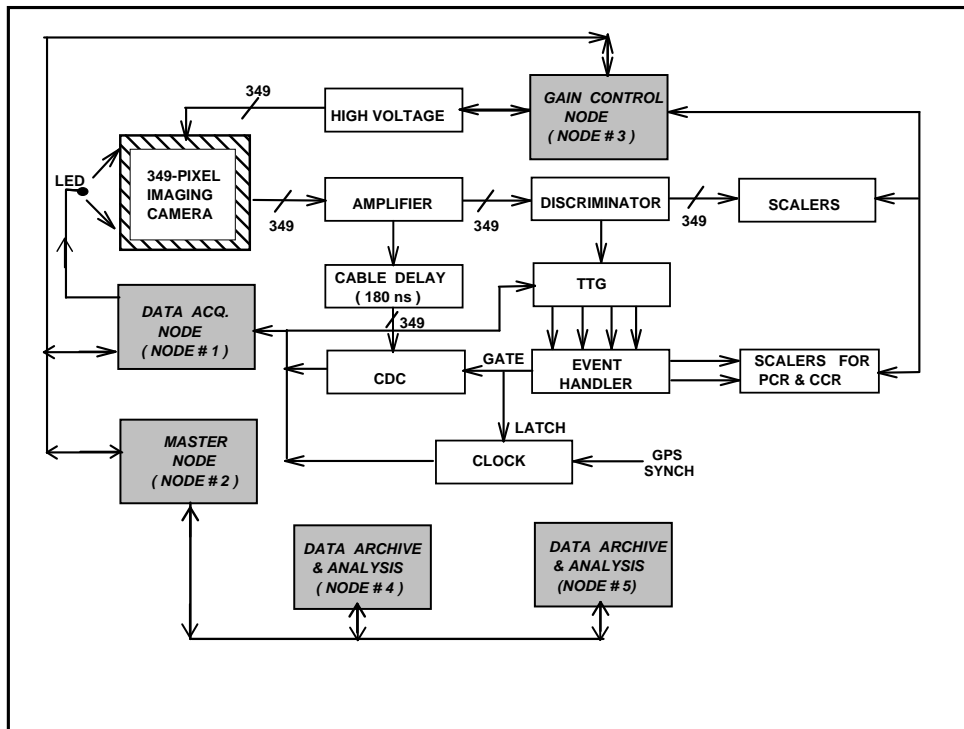


Fig. 6. Block diagram of the back-end signal processing electronics used in the TACTIC imaging element; TTG - TACTIC Trigger generator; PCR-Prompt Coincidence Rate ; CCR- Chance Coincidence Rate.

monitoring the single channel rate with a CAMAC scaler while the other output is connected to the trigger generator for trigger generation. The outputs from each

of the four independently operating trigger generator modules are then collated in an Event Handler which generates the 22ns duration gate pulse and interrupts the data acquisition for reading the charge ADC data from all the 349 pixels. The final trigger pulse is also used for latching the GPS-based clock. The scalers and charge-to-digital converters (CDC) for the 349 channels use 5 CAMAC crates each. Each of these crates is controlled using an in-house developed multicrate CAMAC controller and five such controllers are daisy chained and connected to a data acquisition PC. A similar strategy following a custom built standard has been used for the computer-programmable high voltage units.

7.2 Trigger generation

The imaging camera uses a programmable topological trigger [22] which can pick up events with a variety of trigger configurations. As the trigger scheme is not hard wired, a number of coincidence trigger options (e.g Nearest Neighbour Pairs, Nearest Neighbour Non-collinear Triplets and Nearest Neighbour Non-Collinear Quadruplets) can be generated under software control. The layout of the 349-pixel TACTIC imaging camera, which can use a maximum of 240 inner pixels for trigger generation is depicted in Fig.7a. The trigger criteria have been implemented by dividing these inner 240 pixels into 20 groups of 12 (3×4) pixels. A section of 5 such groups is connected to a TACTIC Trigger Generator (TTG) module and a total of 4 TTGs are required for a maximum of 15×16 matrix of trigger pixels. The trigger scheme has been designed around 16k x 4 bit fast static RAM (Toshiba make TC55B417; access time of < 8 ns). Each of the 4 TTG modules uses 5 memory ICs (indicated by M1-M5 in Fig.7b) and has horizontal cascading built into it. A pictorial representation of the horizontal cascading followed within each trigger generator module is shown in Fig.7b. Vertical cascading has not been provided in the trigger generator due to non-availability of more than 3 outputs from the discriminator. The loss of events as a result of the absence of vertical cascading has been estimated to be about 12% through Monte-Carlo simulations and actual experimentation [23]. The memory address lines are connected to the CAMAC address lines and the front panel receptacles (for connection to the discriminator outputs) through two sets of tri-state buffers. The TTG operation starts with writing of the data, as per a user defined topology, from a disk file into each of its memories under CAMAC control. Once programmed, the TTG outputs follow the event topology as described earlier. Apart from generating the prompt trigger, the trigger generator has a provision for producing a chance coincidence output based on $^{12}C_2$ combinations from various groups of closely spaced 12 channels. This chance coincidence output is used as a system monitor for evaluating its overall functioning during an observation run. Monitoring of the chance coincidence rate has also helped in keeping a close check on the operation of the telescope and the quality of the data collected by it. Other details regarding the design, implementation and performance evaluation of the programmable topological trigger generator for the

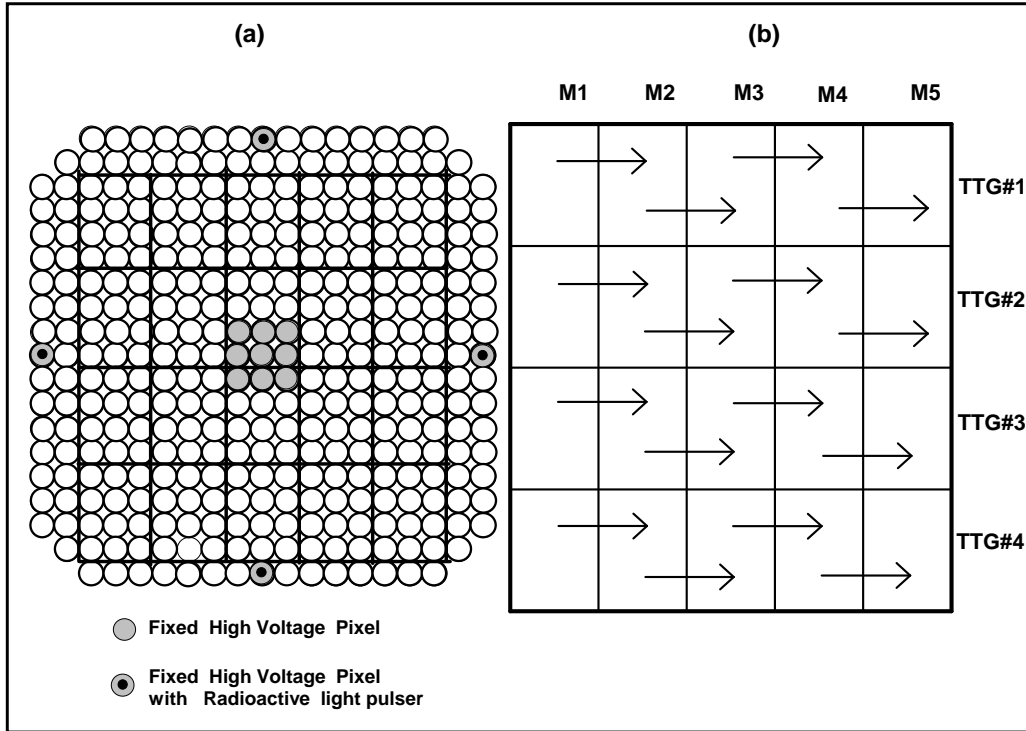


Fig. 7. (a) Layout of the 349-pixel imaging camera of the TACTIC telescope. Shaded pixels in the centre and the same filled with circles at the periphery of the camera represent PMTs for which single channel rate is not stabilized. (b) Pictorial representation of the horizontal cascading followed within each trigger generator module. Each trigger generator module can handle 60 channels by using 5 memory ICs (M1-M5) of type TC55B417.

349-pixel imaging camera of the TACTIC telescope are discussed in [23].

8 Data acquisition and control system

8.1 System architecture

The data acquisition and control system of the telescope has been designed around a network of PCs running the QNX (version 4.25 [24]) real-time operating system. The software is designed for the real time acquisition of event and calibration data and on-line display of telescope status in terms of prompt and chance coincidence rates and the functional status of each of the 349 pixels of the camera. The QNX operating system was chosen for its multitasking, priority-driven scheduling and fast context switching capabilities. In addition, the operating system also provides a powerful set of interprocess communication capabilities via messages, proxies and signals. The data acquisition and control of the TACTIC is handled by

a network of three personal computers as shown in Fig.8. While one PC is used

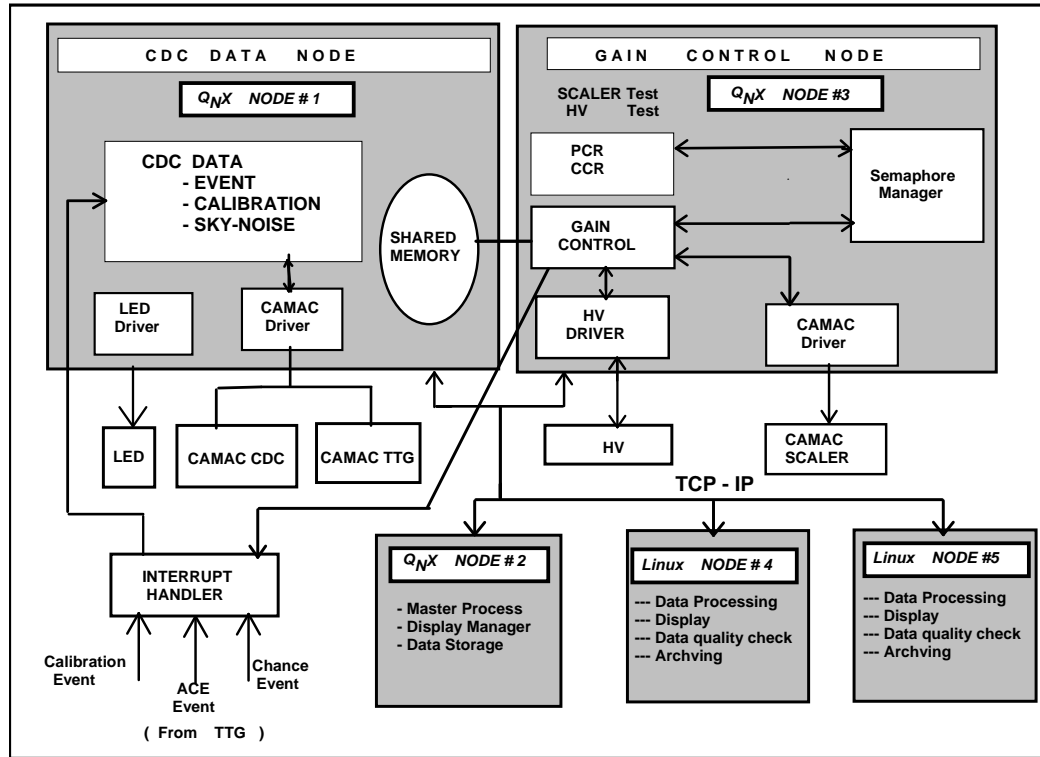


Fig. 8. Block diagram of the multi-node PC-based data acquisition and control system.

to monitor the scaler rates and control the high voltage (HV) to the photomultipliers, the other PC handles the acquisition of the event and calibration data and the programming of the TTGs. These two front-end PCs, referred to as the rate stabilization node and the data acquisition node respectively, along with a master node form the multinode Data Acquisition and Control network of the TACTIC Imaging telescope. All executable routines stored on the master node are spawned on to the other two front-end nodes as and when required. The same network is extended to two more LINUX-based PCs which are used for on-line data analysis and archiving. An event handler module controls the whole process of data acquisition and also provides the link between the TACTIC hardware and the application software. The event handler accepts the atmospheric Cherenkov events, calibration and chance trigger outputs from various TTG modules and interrupts the front end data acquisition node. The system acquires the 349 channel CDC data for the trigger selected atmospheric Cherenkov events, relative calibration flashes generated by the calibration LED and sky pedestal events, in addition to CDC data for the 4 absolute calibration channels. The high voltage and scaler data are also logged continuously, though at a much lower frequency. At event occurrence the event handler also generates a TTL output for latching the system clock and a 20 ns wide NIM pulse for gating the CDC modules. The dead time of the system has been experimentally measured to be ~ 2.5 ms by collecting the relative calibration data along

with absolute time information at a trigger rate of $\sim 400\text{Hz}$. Other details regarding hardware and software features of the data acquisition and control system of the telescope are discussed in [25].

A platform-independent web-based system using the concept of ‘virtual instrumentation console’ is being developed to provide interactive control of the telescope from Mumbai which is about 800 km away from the Mt. Abu observatory. The remote control system will provide location independent access to the data acquisition, control and analysis resources at the observatory using a dedicated 64/128 Kbps ANUNET (Satellite based network) link. The system has two layers with the bottom layer having QNX based telescope data acquisition system linked to WinNT based web server using TCP/IP socket programming. The top layer has java client-server application using servlet communication to provide a rich user interface through standard internet browser. A remote daemon running in the background of the master node will accept connection requests from the web server and once the connection is established it will transmit current status information of the observation run to the remote client. X.509 certification will be used for server and client authentication. The web-server machine will use two network cards and a proxy server installation for internal network security from the outside world. In order to ensure effective utilization of the satellite network bandwidth the data and commands entered by the user on the virtual console will be transmitted to the remote site using very small data volume. Apart from the telescope control the system can also be used for audio-video interactions among the scientists at the two locations.

8.2 *Stabilization of single channel rates*

A cost-effective method for operating the imaging camera of the TACTIC γ -ray telescope at stable single channel rates (SCR) and safe anode current values is being used despite variations in the light of the night sky experienced by the individual pixels from time to time [26]. The camera operates 13 PMTs (9 in the central region and 4 in the periphery of the camera) with fixed high voltages and the remaining 336 pixels at different high voltages to ensure their operation within a pre-determined Single Channel Rate (SCR) range. The purpose behind using the central 9 pixels of the camera at fixed high voltages is to facilitate the gain normalization (flat fielding) of the remaining 336 camera pixels, so that the event sizes (\equiv sum of CDC counts in the clean, flat-fielded image) recorded during a nights observations can be directly compared to one another. Operation of the pixels in a narrow SCR band has the advantage of ensuring a stable chance coincidence rate which can be used as a system diagnostic parameter. An elaborate algorithm [26] has been developed to monitor the SCR rates of all pixels using the CAMAC front ends and ensure their operation within a narrow range despite changes in the background light level incident on them due to changes in the sky brightness and star-field rotation. The

algorithm also ensures that all the pixels of the camera operate within safe anode current ranges. The feedback loop of the algorithm changes the high voltage to the various pixels using multichannel high voltage unit which has a resolution of 1V. The decision of operating a pixel under enhanced light levels is solely based on the comparison of the SCR and applied high voltage with reference data generated under controlled light level conditions. A detailed description of the single channel rate stabilization scheme can be found in [26].

9 Relative and absolute gain calibration scheme

The PMT calibration scheme employed for TACTIC has two parts, viz., relative gain calibration and absolute gain calibration. In the relative gain calibration scheme, we use a high intensity blue LED (Nichia Japan make SPB 500) at a distance of ~ 2 m from the camera to determine the relative gain of the imaging camera pixels. The LED has been provided with a light-diffusing medium in front of it to ensure the uniformity of its photon field within $\sim \pm 6\%$. The mean light intensity from the pulsed LED recorded by each pixel, in response to 2000 light flashes is subsequently used for off-line relative gain calibration of the imaging camera.

The absolute gain calibration system of the camera involves monitoring the absolute gain of a set of 4 gain calibrated pixels (shown by filled circles at the periphery of the camera in Fig.7a). Since measurement of the absolute gains of these PMTs by determining their single photoelectron peaks a number of times during an observation run is rather time consuming, we have instead used a relatively simpler method of measuring the light pulser yield of a calibrated source for the in-situ determination of the absolute gain of these calibration channels. The calibrated light sources used are the Am^{241} -based light pulsers (Scionix Holland BV make; dimensions of YAP:Ce pulser units - 4 mm \times 1 mm) which produce fast optical flashes at an average rate of ~ 20 Hz with maximum emission at a wavelength of ~ 370 nm. After taking several measurements of single photoelectron peak and the radioactive light pulser (RLP) yield under dark room conditions to validate the reproducibility of the measurements and for preparing the reference data base, the PMTs of these calibration channels are mounted permanently with radioactive light pulsers. A collimator is also used during the mounting of a light pulser on a particular tube so that the number of photoelectrons per pulse is ~ 500 pe. These calibration pixels are operated at fixed high voltage values and any changes in the RLP yield measured during actual observations, are then attributed to actual gain change of the pixels. Since the 4 calibration pixels are also partially exposed to the light flashes from the LED during the relative calibration run, it becomes possible to determine the gain of all the pixels of the camera. A representative example of single photoelectron response of one of the PMT's is shown in Fig.9a. The mean amplitude of the single photoelectron peak (indicated by A_{SPE} in Fig.9a) is then determined by fitting a Gaussian distribution function to the differential rate curve. Fig.9b gives

the pulse height distribution of the light flashes obtained with one of the radioactive light pulsers. The underlying principle for converting the charge content of an

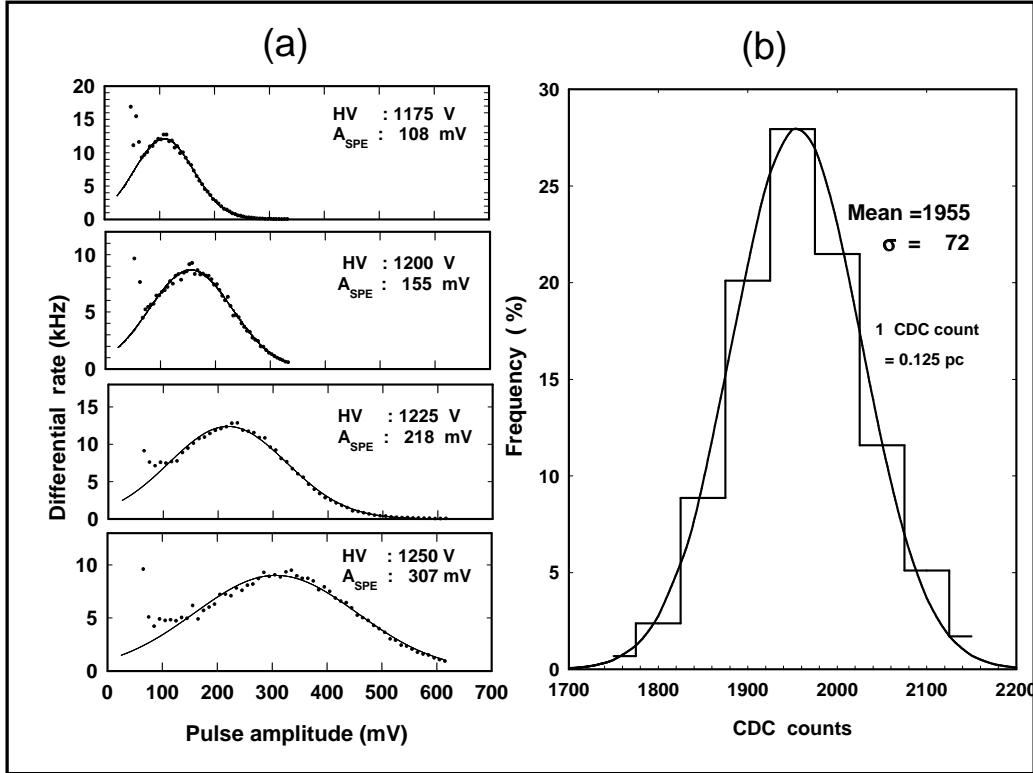


Fig. 9. (a) An example of single photoelectron peak obtained for one of the calibration pixels at different values of HV. (b) Representative example of the pulse height distribution obtained with a Am²⁴¹-based light pulser.

uncalibrated pixel from CDC counts to photoelectrons, uses the fact that the calibration pixels are also exposed to the light flashes from the LED during the relative calibration run and hence it becomes possible to obtain the conversion factors for all the remaining 345 pixels of the camera [27]. The conversion for image size in CDC counts to number of photoelectrons has also been performed independently by using the excess noise factor method. The analysis of relative calibration data yields a value of $1\text{pe} \cong (6.5 \pm 1.2)$ CDC for this conversion factor when an average value of ~ 1.7 is used for excess noise factor of the photomultiplier tubes. Additional work to determine the excess noise factor values more precisely for TACTIC photomultiplier tubes is still underway.

10 Monte Carlo simulations and comparison with real data

10.1 The simulation chain

Due to the non-availability of a calibrated beam of very high energy γ -ray photons, detailed Monte Carlo simulations offer the only way to bench mark the design and performance of an atmospheric Cherenkov imaging telescope. Measurements of absolute γ -ray flux and energy spectra of established γ -ray sources, as well as determination of upper limits on γ -ray emission from quiet objects also rely heavily on Monte Carlo predictions. We have used the CORSIKA (version 5.6211) air shower simulation code [28] for predicting and optimizing the performance of the TACTIC imaging telescope. The complete execution of the Monte Carlo simulations for TACTIC telescope was subdivided into two steps. The first part comprised generating the air showers induced by different primaries and recording the relevant raw Cherenkov data (data base generation). Folding in the light collector characteristics and PMT detector response was performed in the second part. The simulated data-base for γ -ray showers used about 34000 showers in the energy range 0.2-20 TeV with an impact parameter of 5-250m. These showers have been generated at 5 different zenith angles ($\theta= 5^\circ, 15^\circ, 25^\circ, 35^\circ$ and 45°). A data-base of about 39000 proton initiated showers in the energy range 0.4-40 TeV, were used for studying the gamma/hadron separation capability of the telescope. The incidence angle of the proton showers was simulated by randomizing the shower directions in a field of view of $6^\circ \times 6^\circ$ around the pointing direction of the telescope. The Cherenkov photons are ray-traced to the detector focal plane and the number of photoelectrons likely to be registered in a PMT pixel are inferred after folding in the relevant optical characteristics of the mirrors, the metallic compound-paraboloid light concentrator at the entrance window of the pixels and the photocathode spectral response. The Cherenkov photon data-base, consisting of number of photoelectrons registered by each pixel, is then subjected to noise injection, trigger condition check and image cleaning. The resulting data-bases, consisting of pe distribution in the imaging camera at various core distances and zenith angles are then used for estimating (a) trigger efficiency (b) effective detection area (c) optimum ranges of Cherenkov image parameters for discriminating between γ -ray and cosmic ray events (d) differential count rate for γ -ray and cosmic ray events and (e) effective threshold energy of the telescope for γ -ray and cosmic ray proton events. The clean Cherenkov images were characterized by calculating their standard image parameters like LENGTH, WIDTH, DISTANCE, α , SIZE and FRAC2 [10,29]. The standard Dynamic Supercuts [30] procedure was used to separate γ -ray like images from the background cosmic rays. The effective collection area of the telescope, for γ -ray and proton events, at two representative zenith angles values of 15° and 35° is shown in Fig.10a and 10b, respectively. These results were obtained by using the nearest neighbour topological-trigger with 11×11 trigger field and a single pixel threshold of ≥ 25 pe. Fig.10c and 10d show the corresponding differential event

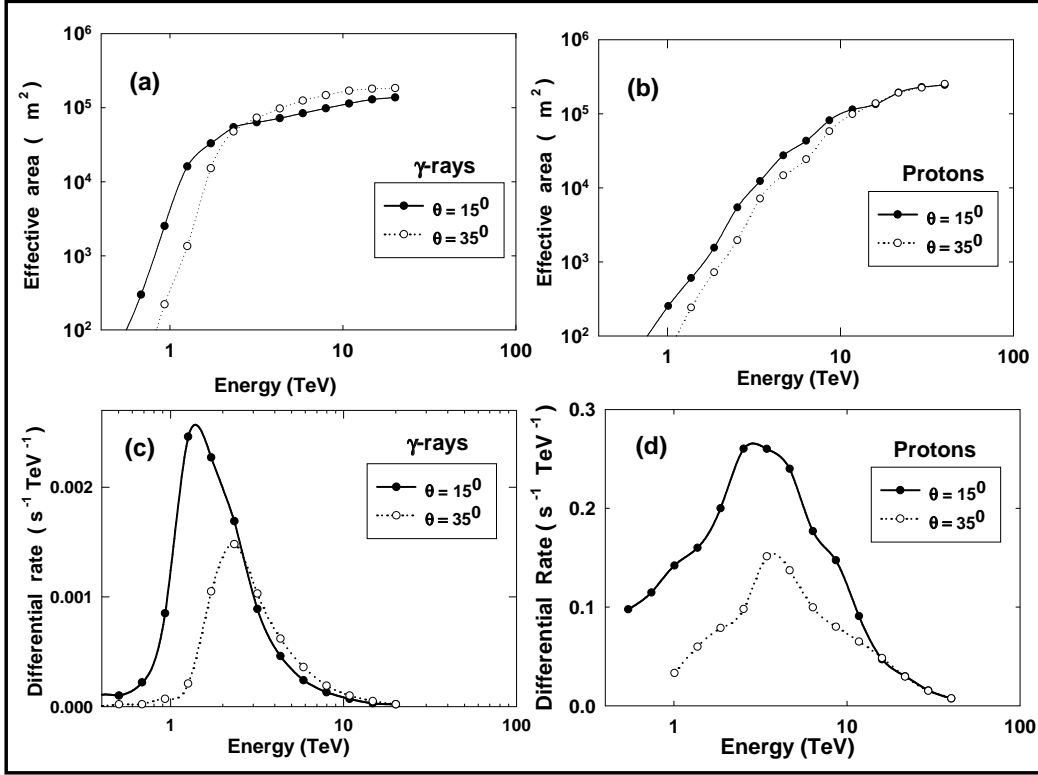


Fig. 10. Effective collection are of the telescope for γ -rays(a) and protons (b) as a function of the primary energy at zenith angles of 15° and 35° . Differential trigger rates for γ -rays (c) and proton events (d) as a function of the primary energy.

rates as a function of the primary energy for γ -ray and proton events, respectively. Defined as the energy where the differential rate peaks and assuming a Crab Nebula type of spectrum with a differential exponent of ~ -2.62 [31], it is evident from Fig.10c that the γ -ray trigger threshold energy of the telescope is ~ 1.2 TeV. The corresponding trigger threshold energy of the telescope for protons turns out to be to ~ 2.5 TeV (Fig.10d).

10.2 Comparison with real data

The agreement between the predictions from Monte Carlo simulations and the actual performance of the telescope was first checked by comparing the observed trigger rate of the telescope with the predicted value. The expected prompt coincidence rate at a zenith angle of 15° turns out to be ~ 2.5 Hz for the nearest neighbour pair trigger mode. This value has been obtained on the basis of integrating the differential rate curve for protons (Fig.10d). Reasonably good matching of this with the experimentally observed value of ~ 2 -3 Hz suggests that the response of the telescope is very close to that predicted by simulations.

The agreement between the expected and actual performance of the telescope was next checked by comparing the expected and observed image parameter distributions. Fig.11 shows the distributions of the image parameters LENGTH, WIDTH, DISTANCE and α [10,29] for simulated protons and for the actual Cherenkov images recorded by the telescope. The simulated distributions of these image parameters for γ -rays have also been shown in the figure for comparison. The observed

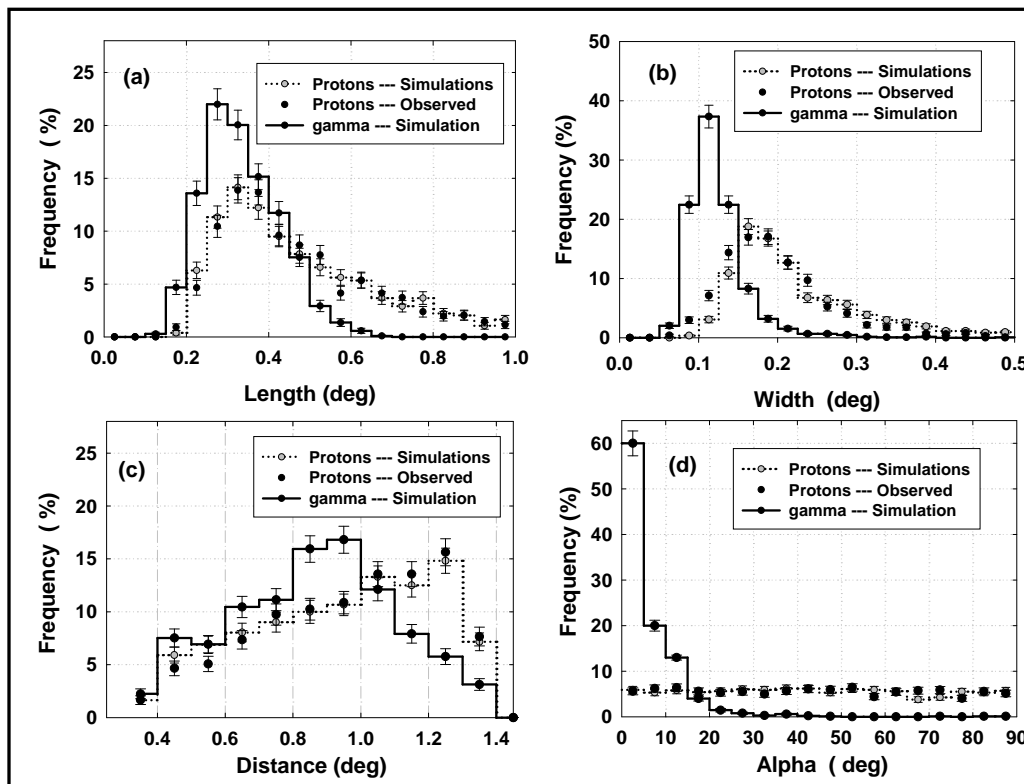


Fig. 11. Comparison of image parameter distributions ((a) LENGTH, (b) WIDTH, (c) DISTANCE and (d) ALPHA) from real and the Monte Carlo simulated data for proton events. The simulated image parameter distribution of γ -rays has also been shown in the figure for comparison.

image parameter distributions are found to closely match the distributions obtained from simulations for proton-initiated showers, testifying to the fact that the event triggers are dominated by background cosmic rays.

A novel ANN (Artificial Neural Network)-based energy estimation procedure for determining the energy spectrum of a candidate γ -ray source has also been developed. The procedure followed by us uses a 3:30:1 (i.e 3 nodes in the input layer, 30 nodes in hidden layer and 1 node in the output layer) configuration of the ANN with resilient back propagation training algorithm to estimate the energy of a γ -ray like event on the basis of its image SIZE, DISTANCE and zenith angle. The new ANN-based energy reconstruction method developed by us, apart from yielding a $\sigma(\ln E)$ of $\sim 28.4\%$, has the added advantage that the procedure allows data collection over a much wider zenith angle range as against a coverage of upto 35° in

case the zenith angle dependence is to be ignored. We have also successfully implemented the ANN-based energy reconstruction algorithm in our analysis chain, by directly using the ANN generated weight-file, so that the energy of a γ -ray like event could be predicted without using the ANN software package. Further results regarding the resulting reconstructed energy spectra of the Crab Nebula and Mrk 421 are presented in the next section.

11 Performance evaluation

The TACTIC telescope with a prototype camera of 81 pixels was made operational in 1997. The telescope was successful in detecting intense TeV γ -ray flaring activity from the BL-Lac object Mkn-501 in the same year. This detection has an important historical significance in the field of very high energy γ -ray astronomy for being the first ever observation of a TeV γ -ray source by 5 independent groups [32]. Since 1997, the TACTIC imaging telescope camera and its data acquisition system has been continuously upgraded. Observations on potential γ -ray sources, however, were continued during this interim period of upgradation phase whenever it became possible. It was during December 2000- March 2001 that the TACTIC imaging telescope in its full configuration of 349 pixels was able to detect γ -rays from the Crab Nebula and another BL -Lac object Mkn-421 at high statistical significances [33]. The results of the Crab Nebula observations, carried out in on/off-source mode (for 41.5 h/30.9 h) between January 19 - February 23, 2001 are shown in Fig.12. The data was taken by using a Nearest Neighbour Non-Collinear Triplets topological trigger with the innermost 240 pixels (15 x 16 matrix) of the camera participating in generating the event-trigger. The 3-fold prompt coincidence rate varied between 3 - 5 Hz. Quite reassuringly, a statistically significant excess of $\sim 6.3\sigma$ is seen in the on-source case (Fig.12a) with respect to the corresponding background level estimated from $20^0 \leq \alpha \leq 65^0$ data. The number of γ -ray like events in the γ -domain ($\alpha \leq 15^0$) turns out to be $\sim 447 \pm 71$. The corresponding off-source α -plot, shown in Fig.12b is in good agreement with the expected flat distribution.

During the last few years regular observations were taken on a number of potential γ -ray sources viz., 1ES2344+514, PSR 0355+54, ON 231, H1426, Mrk-421, Mrk-501 etc. The results of these observations are presented in [34-36]. While we have so far been partially successful in improving the telescope sensitivity by fine-tuning some of the critical parameters, like, the coincidence gate width and the trigger field of view, there is still some scope to improve telescope performance further by making use of better event characterization methodology. At present the telescope has a 5σ sensitivity of detecting Crab Nebula in 25 hours of observation time. This sensitivity figure has been obtained by analyzing recent data on the Crab Nebula for ~ 101.44 h between November 10, 2005 - January 30, 2006 which has yielded an excess of $\sim (839 \pm 89)$ γ -ray events with a statistical significance of $\sim 9.64\sigma$. The data were taken by using the Nearest Neighbour Pair topological trigger with the

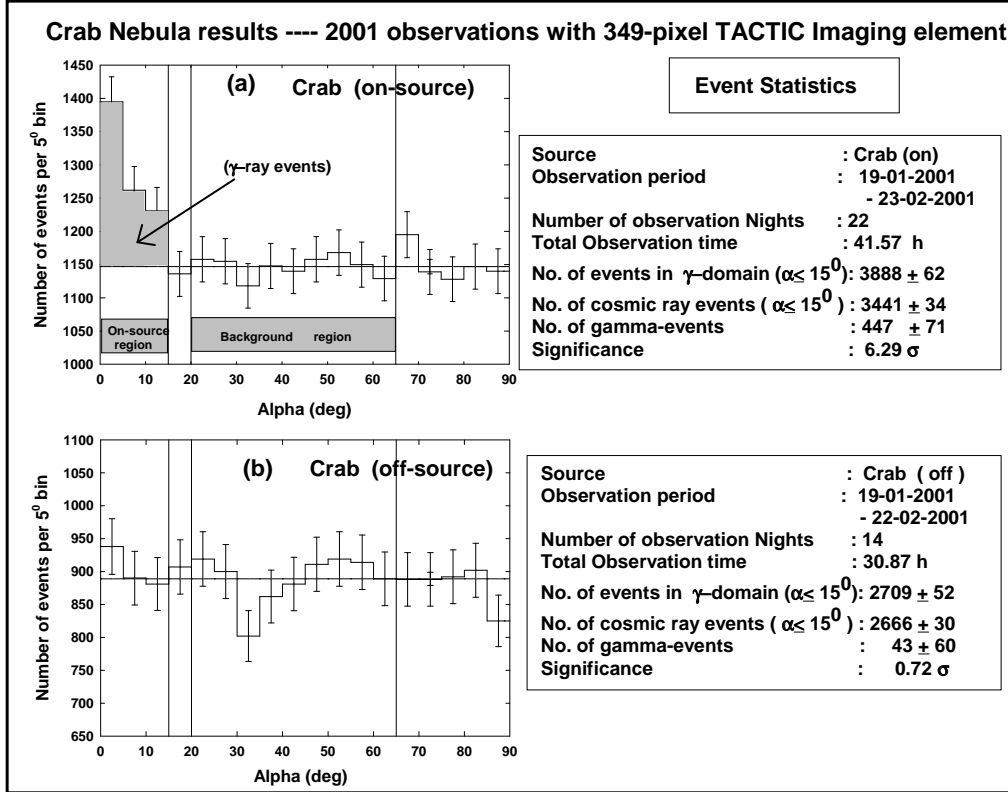


Fig. 12. (a) On-source and (b) Off-source Alpha-plots of the Crab Nebula recorded during January -February 2001 observation spell by 349-pixel TACTIC telescope. The number of γ -ray like events shown in (a) and indicated by the shaded region are found out to be $\sim 447 \pm 71$.

innermost 121 pixels (11 x 11 matrix) of the camera participating in generating the event-trigger. The corresponding average γ -ray rate for the above observations on the Crab Nebula turns out to be $\sim (8.27 \pm 0.88) \text{h}^{-1}$ at γ -ray energies of $\geq 1.2 \text{TeV}$. The differential energy spectrum of the Crab Nebula as measured by the TACTIC telescope is shown in Fig.13a and can be represented by power law ($d\Phi/dE = f_0 E^{-\Gamma}$) with $f_0 = (2.74 \pm 0.19) \times 10^{-11} \text{cm}^{-2} \text{s}^{-1} \text{TeV}^{-1}$ and $\Gamma = 2.65 \pm 0.06$. Excellent matching of this spectrum with that obtained by the HEGRA and Whipple groups [31,37] reassures that the telescope is functioning properly.

Our extensive observations of Mrk 421 on 66 clear nights from December 07, 2005 to April, 30, 2006, totalling ~ 202 hours of on-source observations have also indicated presence of a TeV γ -ray flaring activity from the source [38]. The time-averaged differential γ -ray spectrum in the energy range 1 – 11 TeV is shown in Fig.13b for the data taken between December 27, 2005 to February 07, 2006 when the source was in a relatively higher state as compared to the rest of the observation period. Analysis of this data spell, comprising about ~ 97 h reveals the presence of a $\sim 12.0\sigma$ γ -ray signal with daily flux of > 1 Crab unit on several days. Although not statistically very significant, possible signature of a exponential cut-off in the spectrum at an energy of $\sim (4.7 \pm 2.1) \text{TeV}$ is also seen in Fig.13b. Difficulties like

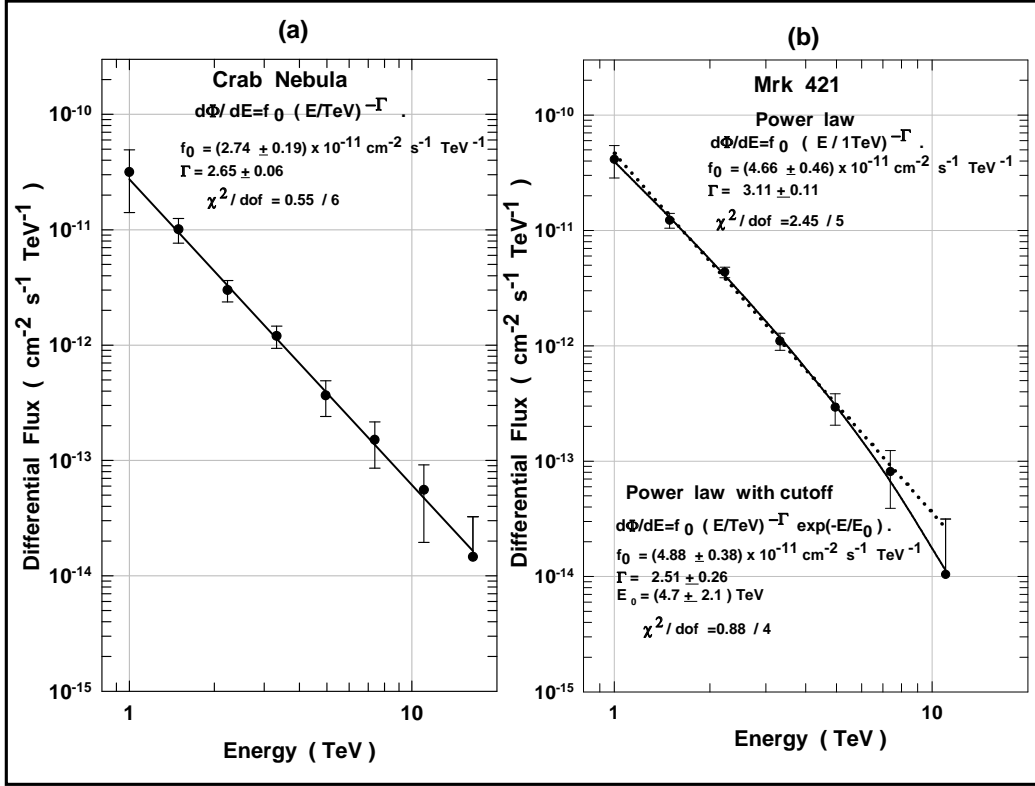


Fig. 13. (a) The differential energy spectrum of the Crab Nebula as measured by the TACTIC telescope. (b) Differential energy spectrum of Mrk 421 for the data collected between December 27, 2005 - February 07, 2006 when the source was in a high state.

limited γ -ray event statistics coupled with rather large error bars do not allow us to claim the cutoff feature at a high confidence level. Other relevant details regarding analysis of the Mrk 421 data, light curve of the source during our observation period and a novel artificial neural network-based energy estimation procedure for determining the energy spectrum of a candidate γ -ray source can be seen in [38].

12 Conclusions

The 349-pixel TACTIC imaging telescope, has been in operation at Mt. Abu, India since 2001 and has so far detected γ -ray emission from the Crab Nebula, Mrk 421 and Mrk 501. While excellent matching of the Crab Nebula spectrum with that obtained by other groups reassures us that the telescope subsystems are functioning properly, the inferred sensitivity level of 1 Crab Unit at $\sim 5.0 \sigma$ in ~ 25 h needs to be further improved. Apart from validating the stability of the TACTIC subsystems directly with γ -rays from this source, matching of the Crab Nebula spectrum also validates the full analysis chain, including the inputs used from the Monte Carlo simulations, like, effective area and γ -ray acceptance factors and the energy re-

construction procedure. Furthermore, keeping in view that the weak signature of possible cutoff energy in the energy spectrum of Mrk 421, inferred from our observations, is fairly consistent with the observations of other groups [39-41], we believe that there is considerable scope for the TACTIC telescope to monitor similar TeV γ -ray emission activity from other active galactic nuclei on a long term basis. Participating in multi-wavelength observation campaigns on various active galactic nuclei and determining the energy spectrum of these sources (both at low average flux levels of < 1 Crab Unit and from intense flares of >2 Crab units) will be one of the main scientific objectives for which the TACTIC telescope will be used during the next few years of its operation. The data collected on these sources will also be utilized to understand the γ -ray production mechanisms of these objects and absorption effects at the source or in the intergalactic medium due to interaction of gamma-rays with the extragalactic background photons [42,43].

13 Acknowledgements

We would like to dedicate this paper to the memory of our departed team leader late Dr. C.L.Bhat who initiated the γ -ray astronomy programme at Mt. Abu but did not live to see it fructify. Unfortunately, he met with a fatal road accident while returning from Mt.Abu on December 17, 2001. The authors would also like to thank colleagues at the Centre for Design and Manufacture, the Electronics Division and Astrophysical Sciences Division of our centre who have contributed during the various stages of the planning, fabrication, installation and operation of the telescope. We would like to thank Dr.V.G.Sinitsyna and other colleagues from the P.N.Lebedev Institute, Moscow for many useful discussions and also for providing us the design details of the SHALON telescope.

References

- [1] F.Aharonian et al., *Astron. Astrophys.*, 370 (2001) 112.
- [2] F.Aharonian et al., *Astron. Astrophys.*, 449 (2006) 223.
- [3] F.Aharonian et al., *Astron. Astrophys.*, 393 (2002) 371.
- [4] F.Aharonian et al., *Astron. Astrophys.*, 442 (2005) 1.
- [5] J.Albert et al., *Science*, 312 (2006) 1771.
- [6] D.Horan and T.C.Weekes, *New Astron. Rev.*, 48 (2004) 527.
- [7] F.Aharonian et al., *Nature*, 440 (2006) 1018.
- [8] T.C.Weekes, *Phys. Rep.*, 160 (1988) 1.

- [9] A.Daum et al., *Astropart. Phys.*, 8 (1997) 1.
- [10] A.M.Hillas, *Proc. 19th ICRC*, La Jolla, 3 (1985) 445.
- [11] D.J. Fegan, *Space Science Reviews*, 75 (1996) 137.
- [12] E.Lorentz et al., *New Astron. Rev.*, 48 (2004) 339.
- [13] T.C.Weekes et al., *Astropart. Phys.*, 17 (2002) 221.
- [14] J.A.Hinton et al., *New Astron. Rev.*, 48 (2004) 331.
- [15] H.Kubo et al., *New Astron. Rev.*, 48 (2004) 323.
- [16] C.L. Bhat, *Proc. Perspectives in High Energy Astronomy and Astrophysics*, Mumbai, India, 1996, p384.
- [17] R.K.Kaul et al., *J.Astrophys. Astr.*, 15 (1994) 95.
- [18] S.K.Kaul et al., *Meas. Sci. Technol.*, 8 (1997) 329.
- [19] A.K.Tickoo et al., *Exp. Astron.*, 9 (1999) 81.
- [20] A.K.Tickoo et al., *Nucl. Instr. and Meth. A*, 539 (2005) 177.
- [21] C.L.Bhat et al., *Meas. Sci. Technol.*, 7 (1996) 706.
- [22] C.L.Bhat et al., *Nucl. Instr. and Meth. A*, 340 (1994) 413.
- [23] S.R.Kaul et al., *Nucl. Instr. and Meth. A*, 496 (2003) 400.
- [24] QNX System Architecture by QNX Software Systems Ltd., www.qnx.com
- [25] K.K.Yadav et al., *Nucl. Instr. and Meth. A*, 527(2004) 411.
- [26] N.Bhatt et al., *Meas. Sci. Technol.*, 12 (2001) 167.
- [27] A.K.Tickoo et al., *Bull. Astr. Soc. India*, 30 (2002) 381.
- [28] D.Heck et al., *Report FZKA 6019 Forshungszentrum, Karlshrue*, (1998).
- [29] T.C.Weekes et al., *Ap.J*, 342 (1989) 379.
- [30] G.Mohanty et al., *Astropart. Phys.*, 9 (1998) 15.
- [31] F.Aharonian et al., *Ap.J*, 614 (2004) 897.
- [32] R.J.Protheroe et al., *Proc. 25th ICRC*, Kruger Park, South Africa, 8 (1997) 317.
- [33] N.Bhatt et al., *Bull. Astr. Soc. India*, 30 (2002) 385.
- [34] S.V.Godambe et al., *J.Phys. G : Nucl. Part. Phys.*, 34 (2007) 1683.
- [35] S.Thoudam et al., *Proc. 29th ICRC*, Pune, India, 4 (2005) 363.
- [36] R.C.Rannot et al., *Proc. 29th ICRC*, Pune, India, 4 (2005) 355.
- [37] A.M.Hillas et al., *ApJ*, 503 (1998) 744.

- [38] K.K.Yadav et al., *Astropart. Phys.*, 27 (2007) 447.
- [39] F.Krennrich et al., *Ap.J*, 560 (2001) L45.
- [40] F.Aharonian et al., *Astron. Astrophys.*, 410 (2003) 813.
- [41] F.Aharonian et al., *Astron. Astrophys.*, 437 (2005) 95.
- [42] A.Konopelko et al., *Ap.J*, 597 (2003) 851.
- [43] E.Dwek and F.Krennrich, *Ap.J*, 618 (2005) 657.